Effect of Pinning on the Yielding Transition of Amorphous Solids

Bhanu Prasad Bhowmik,[1] Pinaki Chaudhuri,[2] and Smarajit Karmakar[1,*]
[1]Tata Institute of Fundamental Research, 36/P, Gopanpally Village, Serilingampally Mandal, Ranga Reddy District, Hyderabad, 500107, Telangana, India
[2]Institute of Mathematical Sciences, IV Cross Road, CIT Campus, Taramani, Chennai, 600113, Tamil Nadu, India

(Received 8 September 2018; published 29 October 2019)

Using numerical simulations, we have studied the yielding response, in the athermal quasistatic limit, of a model amorphous material having inclusions in the form of randomly pinned particles. We show that, with increasing pinning concentration, the plastic activity becomes more spatially localized, resulting in smaller stress drops, and a corresponding increase in the magnitude of strain where yielding occurs. We demonstrate that, unlike the spatially heterogeneous and avalanche led yielding in the case of the unpinned glass, for the case of large pinning concentration, yielding takes place via a spatially homogeneous proliferation of localized events.

DOI: 10.1103/PhysRevLett.123.185501

Introduction.—A systematic understanding of microscopic processes that lead to yielding of amorphous solids is still missing [1–3]. It has been demonstrated that the elementary events that build up to yield correspond to local plastic activity within a shear transformation zone, whereby a small set of particles undergo irreversible structural rearrangement [4]. Starting from an initially quiescent glassy state, shear initially induces few such plastic events, which proliferate with increasing deformation; after some strain, the system fails to resist applied shear and starts to yield and rupture (brittle) or flow (ductile). Recently, it was predicted [5,6] and subsequently demonstrated in metallic glasses [7], that yielding via a brittle or ductile response can be achieved by the degree of annealing undergone during glass formation. Similar conclusions were also obtained in the study of model computer glasses [8], by tuning of stability via annealing, where it is suggested that the ductile rupture corresponds to a first-order nonequilibrium transition.

Most theoretical studies probing the yielding transition have worked in the athermal quasistatic limit, which mimics the deformation of the system at zero temperature and strain rate $\dot{\gamma} \to 0$ [1]. It has been evidenced that the stress released during plastic activity results in a cascade of events leading to catastrophic system spanning avalanches [9,10]. Following yield from the quiescent state, across the plastic rearrangements in steady state, a power law dependence of energy drops (ΔU) and stress drops ($\Delta\sigma$) on system size (N) is reported: $\Delta U \sim N^{\alpha}$ and $\Delta\sigma \sim N^{\beta}$, where these exponents are found to have universal value $\alpha = 1/3$ and $\beta = -2/3$, irrespective of model and spatial dimensions [11], which, however, has been scrutinized recently [12] and perhaps a clear consensus is yet to emerge. The scale-free nature of these avalanches indicates some type of criticality in the yielding process [8,13–18], manifestng itself as spinodal point of an underlying thermodynamic phase transition, described by an appropriate replica "order parameter" (see also Refs. [8,15,16,18]). Exploration of such critical behavior has also been extended to the regime of finite, but small, shear rates [12,19–21] and finite temperatures [22].

In this Letter, we probe the quasistatic elastoplastic behavior of the amorphous solid, altered by the presence of tiny inclusions, in the form of pinned particles. Recently, such random pinning has been found to be an interesting tool to test different theories of glass transition and for probing the growth of static structural order in the system [23–31], and also to study the non-Debye low-frequency excitations in glasses [32]. For our present study of the shear response, we consider the case where the tiny inclusions undergo affine deformation when the macroscopic solid is deformed, but do not have any nonaffine motion. While it is historically known that such inclusions strengthen a material [33–36], a systematic statistical study of yielding and its microscopic ramifications is still missing, except for some investigations via mesoscale or continuum models [37,38]. Thereby, it can potentially provide microscopic insight into industrially relevant cases like micro-alloying in metallic glasses [39–42], or nanoparticles in soft matrices.

Our work shows that as the solid becomes more and more rigid, with increase in the concentration of pinned particles, the initiation of plastic activity gets delayed too, and thereby the strain at which yielding occurs systematically shifts to higher values. The drop in stresses, corresponding to plastic activity, also become smaller in scale, with increased concentration, suggesting localized relaxation processes. Consequently, the stress statistics reveal that drop sizes change from subextensive to intensive in system size, with increasing pinning concentration. Therefore, in

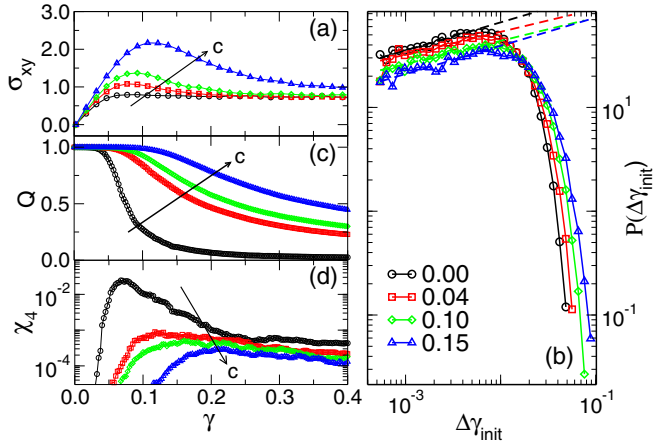

FIG. 1. Yielding—macroscopic monitoring. (a) Evolution of shear stress, σ_{xy} with strain γ, for pinning concentrations $c = 0.00, 0.04, 0.10, 0.15$, in $d = 2$. The direction of increasing c is marked with an arrow. (b) Distribution of $\Delta\gamma_{\text{init}}$, the strain interval between two successive stress drops, during transient response from the quiescent state, and corresponding fits (dashed lines) to extract the exponent θ of the Weibull distribution. (c) Related evolution of overlap function $Q(\gamma)$ computed over an ensemble of initial states and (d) related fluctuations, $\chi_4(\gamma)$. The location of the maxima indicates the yield point (γ_Y).

contrast to large-scale spatially heterogeneous avalanches, as has been observed in usual amorphous systems, for pinned systems, the yielding occurs via the homogeneous accumulation of localized plastic activity.

Model and method.—For our study, we consider the Kob-Andersen model in two and three dimensions [43]. The details of the model and the protocol for preparing the annealed glasses, the inherent structure states, as well as the pinning protocol are provided in the Supplemental Material [44]. The mechanical response of both pinned and unpinned states are studied using the athermal quasistatic shear (AQS) protocol. Data shown here correspond to $d = 2$, unless otherwise specified. See Ref. [44] for corresponding data related to $d = 3$.

Macroscopic scenario of yielding from quiescent state.—We first illustrate the macromechanical response via the evolution of the shear stress (σ_{xy}) with increasing applied strain (γ) for $N = 4000$ particles, and for different concentrations of pinning (c), shown in Fig. 1(a), with averaging being done over different realizations of random pinning, for each value of c. Initially, the stress increases linearly with strain, followed by an intermediate regime of nonlinear response, before eventually large scale plasticity sets in and the system reaches long-time steady flow. For the case of unpinned glass, there is not much of a stress overshoot, prior to the onset of steady flow, as is the usual case in most moderately annealed glasses [8]. However, as the pinning concentration is increased, a stress overshoot appears and the stress peak increases with increasing c, with the location of the peak occurring, also, at larger values of strain. Meanwhile, at small strain, the slope of the σ_{xy} vs γ curve, is observed to be more steep, indicating that the pinning is making the solid more rigid leading to increase in the shear modulus [35].

This increased rigidity with pinning is also reflected in the distribution of the strain interval to first stress drop, $\Delta\gamma_{\text{init}}$, when quiescent glassy states are sheared [11]. As shown in Fig. 1(b), for different c values, the probability of the first plastic drop occurring at small strain decreases, with increasing c, and more weight is transferred to larger strain intervals, demonstrating that the system becomes more stable with increased pinning. We have fitted $P(\Delta\gamma_{\text{init}})$ using Weibull distribution [51], $W(x) = Ax^{\theta}\exp[-(x/x_0)^{1+\theta}]$ to extract the exponent θ, obtaining $\theta \approx 0.35$ for all explored pinning concentrations; see Ref. [44] for further details.

To quantitatively identify the value of the yield strain, we compute the fluctuation, $\chi_4(\gamma)$, of the overlap function $Q(\gamma)$, over the ensemble of initial states, for different values of c (see Ref. [44] for details). For each c, $Q(\gamma)$ is computed in reference to each initial quiescent state within the corresponding ensemble. The average $Q(\gamma)$ [see Fig. 1(c)] computed over the independent trajectories starting from these initial states shows that the structural relaxation slows down with increasing pinning. The corresponding curves for $\chi_4(\gamma)$ vs γ [see Fig. 1(d)] has a nonmonotonic behavior for all values of c and the location of the maximum is identified as the strain threshold (γ_Y) at which the system yields [8], thereby quantitatively evidencing that γ_Y increases with increasing pinning concentration. Note that the scale of fluctuations [i.e., peak height of $\chi_4(\gamma)$] decreases with c, reflecting that pinning exerts constraints on the possible explorable states [52].

Macroscopic steady-state response.—We now characterize the steady-state flow properties of these systems. Typical time series of the stress, in steady state, for a single trajectory, is shown in the inset of Fig. 2(a), for $c = 0$

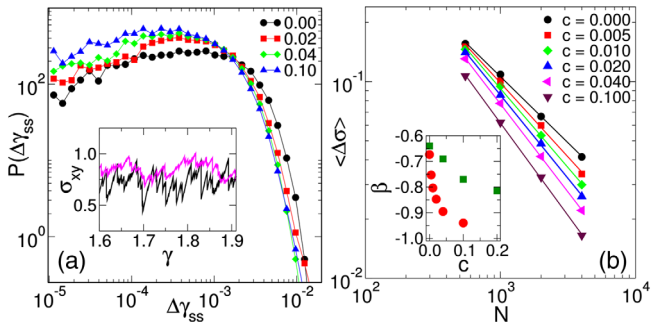

FIG. 2. Steady-state macroscopic behavior. (a) Distribution of $\Delta\gamma_{\text{ss}}$, the strain interval between two successive stress drops during steady state. (Inset) Stress vs strain curves for the unpinned ($c = 0$) and pinned ($c = 0.15$) cases. (b) Finite size effects in stress drops ($\langle\Delta\sigma\rangle \sim N^{\beta}$), for varying pinning concentrations (c) in $d = 2$. (Inset) Corresponding evolution of exponent β with c, for $d = 2$ (circles), 3 (squares).

and finite c: for the unpinned case, the stress drops have the well-known sawtooth profile [1], and for increasing pinning, the stress drops become visibly smaller. If we consider the probability distribution of $\Delta\gamma_{ss}$, the strain gap between two consecutive plastic drops in the steady state, we observe [see Fig. 2(a)] that the probability of having plastic events within small $\Delta\gamma_{ss}$ increases with increasing pinning concentration, whereas the probability of larger $\Delta\gamma_{ss}$ between stress drops decreases. This suggests that, in the steady state, the system has a strong tendency to have many small plastic drops instead of large system spanning avalanches. Note that this observation is contrary to the idea that pinning effectively makes the system size smaller. For smaller system size, one expects on average $\langle\Delta\gamma_{ss}\rangle$ to be larger compared to bigger system size, which is very different with increasing pinning concentration, where the number of drops increase rather than decrease.

We have also analyzed the steady-state statistics of drops in shear stress $\langle\Delta\sigma\rangle$ for the different c, with varying system size N, via $\langle\Delta\sigma\rangle \sim N^{\beta}$; see Fig. 2(b). For the unpinned system, the exponent β is known to be universal, viz. $\beta = -2/3$ [11]. In Fig. 2(b) inset, β vs c is plotted for $d = 2, 3$ [44], which show the strong dependence on pinning concentration: in $d = 2$, β goes from $-2/3$ to approximately -1.0 with a 20% increase in c, whereas in $d = 3$, it decreases to approximately -0.8, for the same increase in c, since more paths for percolation are available in $d = 3$. Thus, stress drops are becoming subextensive to intensive, indicating that pinning does affect the avalanching process.

Microscopic steady-state response.—We now investigate how the mechanical response manifests at the microscopic scale, by studying nonaffine displacement fields generated during stress drops. In the top panel of Fig. 3, we show examples of the displacement fields generated during stress drops in steady flow, for two contrasting cases, viz. $c = 0$ (a) and $c = 0.1$ (b), using $N = 10000$. For the unpinned case, a large stress drop corresponds to large scale displacements, in the form of a system-spanning avalanche, as has been observed and well studied [1,2,9,10]. However, for $c = 0.1$, we see that the spatial scale of the region, undergoing large displacements, is completely localized. The spatial correlations in such displacement fields are measured, which clearly show that with increasing c, a cutoff scale appears and the nature of the correlation function changes from power law ($c = 0$) to power law with exponential cutoff (see Supplemental Material [44] for details), from which one can extract a correlation length ξ for each c [see Fig. 3(c)], capturing the increased localization of plastic activity with increasing c. This confirms that the propagation of stress gets hindered due to the presence of the pinning centers and thereby the avalanche-like character of the nonaffine displacements, during a stress drop, is progressively cut off with increased pinning.

This observation is further quantified by identifying the particles that are part of the relaxation process during the stress drop and measuring the corresponding cluster size (S). In order to label a particle as mobile, we only consider those that move more than some threshold distance during the stress drop, by analyzing the probability distribution of displacements of particles during plastic events, which show power law behavior with an exponential tail (see Ref. [44] for details). We compute the distribution of cluster size $P(S)$ for both pinned and unpinned cases. The distribution for $c = 0$ [Fig. 3(d)] shows a power law behavior $P(S) \sim S^{-1.5}$ with a hump at large cluster size, which indicates the presence of a percolating cluster, and the corresponding S scales with the system size (N) (See the Supplemental Material for detailed discussion). For higher pinning concentration, the range of power law decreases and shows no hump at large cluster size (see Ref. [44]) and the distributions do not show any size effect [Fig. 3(e)]. On the other hand, a rescaling with the correlation scale $\xi(c)$ seems to provide a reasonable data collapse [see Fig. 3(f) and also discussion in the Supplemental Material [44]]. Thus, via all these statistical analyses, we can conclude that system spanning avalanches start to become less frequent with increasing pinning

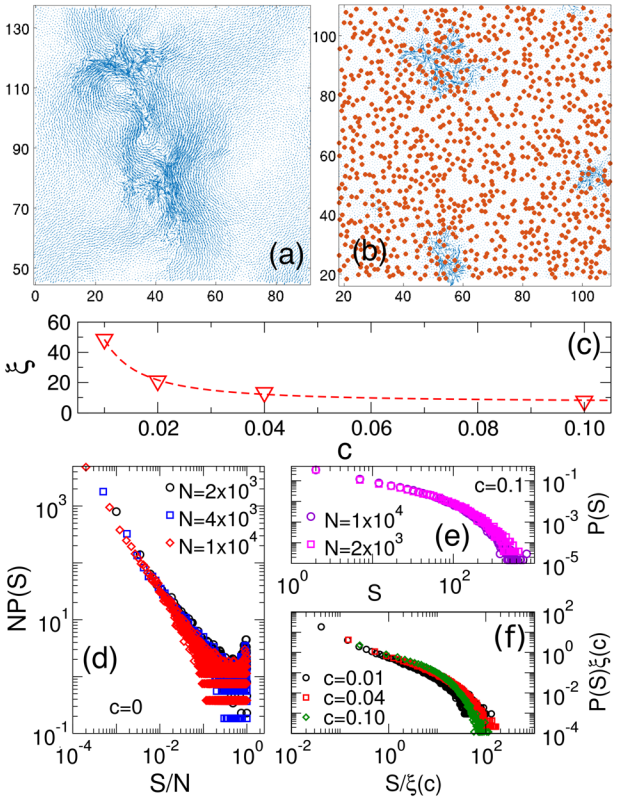

FIG. 3. Microscopic steady-state scenario. Displacement field during a single large stress drop, for (a) $c = 0.0$, (b) $c = 0.1$. (c) Variation of correlation length (ξ), with c, within the displacement field. (d) $c = 0$: scaling of distribution of cluster size, $P(S)$, with system size N. (e) $c = 0.1$: Variation of $P(S)$ with N. (f) Data collapse of data for $P(S)$, for $c \neq 0$, via rescaling with $\xi(c)$.

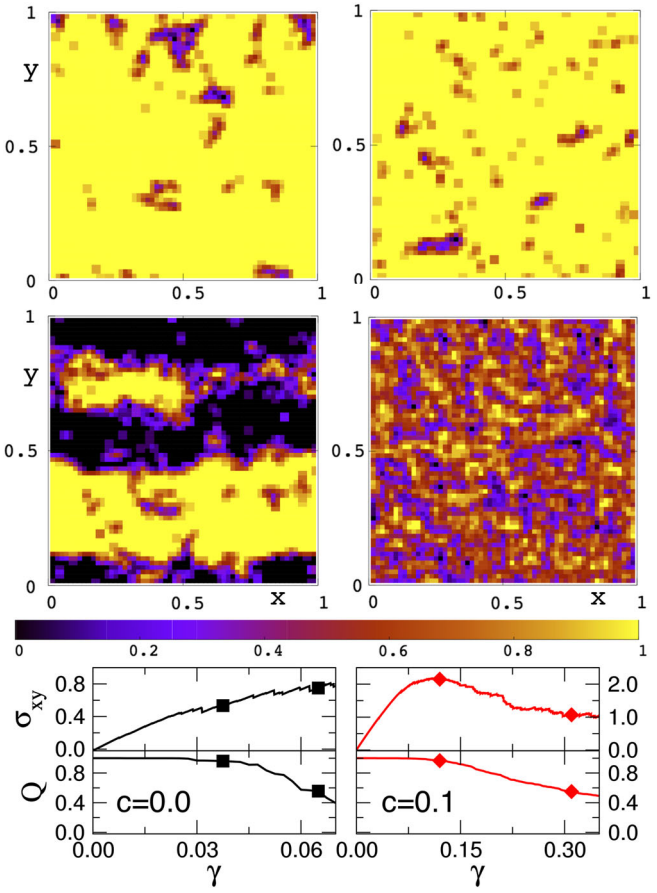

FIG. 4. Microscopics of yielding. $N = 10000$. Sequence of maps of local overlap $\tilde{Q}(x, y)$ during yielding, for (left) $c = 0$, shown for strain values of 0.0375 (top), 0.0650 (bottom) and (right) for $c = 0.10$, shown for strain values of 0.12 (top), 0.31 (bottom). The color bar shows the scale of local overlap in each case. Corresponding evolution of macroscopic stress (σ_{xy}) and also global overlap function (Q), with increasing strain, are shown in the bottom panels. See Ref. [44] for further information and animations.

concentration and beyond a certain pinning concentration, the avalanchelike cascade of plastic rearrangements completely disappear, and localized events determine plastic behavior.

Microscopic scenario for yielding.—We now microscopically analyze how stress drops, and, consequently, particle displacements lead to yielding and eventual large scale flow. To monitor this, we construct maps of local overlap, $\tilde{Q}(x, y)$ [44], relative to the initial quiescent state, and follow how the map evolves as a function of increasing strain, for the pinned and unpinned cases. This evolution is shown in Fig. 4, for a trajectory from either case, for $N = 10000$. Additionally, we show the corresponding evolution of shear stress (σ_{xy}) and overlap (Q) with strain. For the unpinned case, shown in the left column of Fig. 4 (see also Supplemental Material, animation [44]), at early strains, we have the first plastic events, occurring at small scale, at different spatial locations. As strain increases, more such events occur, with some of the relaxed regions (which, now, have lower local overlap relative to the initial state) increasing in scale; i.e., they become nuclei of yielding in their neighborhood. Eventually these regions connect, avalanches occur, and the relaxed parts span the system; i.e., there is a percolation of mobile regions [22]. Importantly, one sees spatial localization of mobility in the form of bands spanning the system in the shear direction, the width of which increase with increasing strain [53]. To summarize, in this case, the states, transient to complete fluidization, correspond to avalanches and flow heterogeneities.

This contrasts with the case of pinned states, considering the example of $c = 0.1$, where we have shown that stress drops lead to localized plasticity and not avalanches. The corresponding maps of local overlap are shown in the right panel of Fig. 4 (also see Supplemental Material, animation [44]). Here, the first visible signs of plastic activity occur at larger strain, since the pinning has rendered the system more rigid. With increasing strain, these regions start to grow in number. This is in contrast to the unpinned case, where the initial regions were driving increased plasticity, in their neighborhood. In the case of pinned particles, since plasticity is localized, nonlocal effects are screened, which lead to more regions locally yielding. Because of such a scenario, these spots pop up in a spatially homogeneous manner, and no system-spanning events are observed. Thus, at larger strain, yielding happens via the homogeneous occurrence of such small-scale localized activities, filling up the entire system. We note the contrasting spatial picture for the two systems, at the right-most end of the two panels, which both have the same global overlap value ($\approx$0.57). Further, we also note here, that even though there is a prominent stress overshoot, for $c = 0.1$, and that too in the vanishingly small shear-rate limit, no flow heterogeneities are observed in this case, as has often been conceived [54].

To summarize, we have studied the shear response of amorphous solids, in the quasistatic limit, with pointlike inclusions embedded within them. The significant finding is that, with increasing concentration of inclusions, yielding gets delayed as the initiation of plastic activity becomes difficult with the local constraints imposed by the pinned particles. One would assume that the local yielding thresholds [55] get altered with the presence of these inclusions, leading to this hindrance. Further, even when plastic events occur, the propagation of the stress relaxation across the system is cut off by the inclusions, leading to localized dissipation in the form of smaller stress drops, which is very different from the avalanchelike dissipation in the unpinned amorphous solid. From the generated displacement fields and their spatial correlations, it is clear that the stress propagator which has the long-ranged Eshelby form for the unpinned solid, gets more and more spatially

screened with increasing pinning concentration and therefore the modified form needs to be calculated, to develop appropriate mesoscale description [56] for the ensuing yielding scenario. Finally, we have brought together these different elastoplastic aspects to illustrate how yielding and subsequent plasticity proceeds, starting from a quiescent state. Distinct from the spatially heterogeneous initiation of large scale plasticity in the unpinned amorphous solid, the presence of the inclusions leads to a more spatially homogeneous yielding, with the different zones of activity likely to be more decoupled and toppling independently. Thus, even though there is increased rigidity due to inclusions, there are no brittlelike ruptures with accompanying shear bands as found in ultrastable glasses [8]. Note that while pinning does not impact the energy levels of inherent structures, rather a particular pinning construction localizes the system in a particular metabasin within the landscape [57,58]. On the other hand, slower annealing leads to reaching lower energy levels. Thus, the relaxation paths and thereby the mechanical response in the two cases can be very different in the two cases. How this scenario influences the rheology at finite shear rates [12,21,59] remains to be investigated. Further, motivated by these results, we have explored [44] how inclusions in the form of large particles, which would have relatively smaller nonaffine motion under shear, can not only tune the rigidity, but also have more homogeneous yield mechanism, demonstrated in this work. Such studies have the potential for developing soft matter systems or microalloys, which can continue to be ductile, even when seeded with inclusions to increase toughness.

We would like to thank Surajit Sengupta, Jürgen Horbach, Jean-Louis Barrat, Kirsten Martens, Sanat Kumar, and Srikanth Sastry for useful discussion. We would also like to thank Anoop Mutneja for various help and discussion.

*smarajit@tifrh.res.in

[1] J.-L. Barrat and A. Lemaitre, Heterogeneities in amorphous systems under shear, *Dynamical Heterogeneities in Glasses, Colloids, and Granular Media* (Oxford University Press, Oxford, 2011), Vol. 150, p. 264.
[2] D. Rodney, A. Tanguy, and D. Vandembroucq, Model. Simul. Mater. Sci. Eng. **19**, 083001 (2011).
[3] D. Bonn, M. M. Denn, L. Berthier, T. Divoux, and S. Manneville, Rev. Mod. Phys. **89**, 035005 (2017).
[4] M. L. Falk and J. S. Langer, Phys. Rev. E **57**, 7192 (1998); Annu. Rev. Condens. Matter Phys. **2**, 353 (2011); J. S. Langer, Phys. Rev. E **77**, 021502 (2008).
[5] C. H. Rycroft and E. Bouchbinder, Phys. Rev. Lett. **109**, 194301 (2012).
[6] M. Vasoya, C. H. Rycroft, and E. Bouchbinder, Phys. Rev. Applied **6**, 024008 (2016).
[7] J. Ketkaew, W. Chen, H. Wang, A. Datye, M. Fan, G. Pereira, U. D. Schwarz, Z. Liu, R. Yamada, W. Dmowski, M. D. Shattuck, C. S. O'Hern, T. Egami, E. Bouchbinder, and J. Schroers, Nat. Commun. **9**, 3271 (2018).
[8] M. Ozawa, L. Berthier, G. Biroli, A. Rosso, and G. Tarjus, Proc. Natl. Acad. Sci. U.S.A. **115**, 6656 (2018).
[9] A. Tanguy, Fabien Leonforte, and J.-L. Barrat, Eur. Phys. J. E **20**, 355 (2006).
[10] C. E. Maloney and A. Lemaitre, Phys. Rev. E **74**, 016118 (2006).
[11] S. Karmakar, E. Lerner, and I. Procaccia, Phys. Rev. E **82**, 055103(R) (2010).
[12] J. Lin, E. Lerner, A. Rosso, and M. Wyart, Proc. Natl. Acad. Sci. U.S.A. **111**, 14382 (2014).
[13] C. Rainone, P. Urbani, H. Yoshino, and F. Zamponi, Phys. Rev. Lett. **114**, 015701 (2015).
[14] C. Rainone and P. Urbani, J. Stat. Mech. (2016) 053302.
[15] G. Biroli and P. Urbani, SciPost Phys. **4**, 020 (2018).
[16] G. Parisi, I. Procaccia, C. Rainone, and M. Singh, Proc. Natl. Acad. Sci. U.S.A. **114**, 5577 (2017).
[17] I. Procaccia, C. Rainone, and M. Singh, Phys. Rev. E **96**, 032907 (2017).
[18] Y. Jin, P. Urbani, F. Zamponi, and H. Yoshino, Sci. Adv. **4**, eaat6387 (2018).
[19] A. Lematre and C. Caroli, Phys. Rev. Lett. **103**, 065501 (2009).
[20] K. M. Salerno and M. O. Robbins, Phys. Rev. E **88**, 062206 (2013).
[21] C. Liu, E. E. Ferrero, F. Puosi, J. L. Barrat, and K. Martens, Phys. Rev. Lett. **116**, 065501 (2016).
[22] G. P. Shrivastav, P. Chaudhuri, and J. Horbach, Phys. Rev. E **94**, 042605 (2016).
[23] C. Cammarota and G. Biroli, Proc. Natl. Acad. Sci. U.S.A. **109**, 8850 (2012).
[24] W. Kob and L. Berthier, Phys. Rev. Lett. **110**, 245702 (2013).
[25] M. Ozawa, W. Kob, A. Ikeda, and K. Miyazaki, Proc. Natl. Acad. Sci. U.S.A. **112**, 6914 (2015).
[26] S. Chakrabarty, S. Karmakar, and C. Dasgupta, Sci. Rep. **5**, 12577 (2015).
[27] S. Chakrabarty, S. Karmakar, and C. Dasgupta, Proc. Natl. Acad. Sci. U.S.A. **112**, E4819 (2015).
[28] R. Das, S. Chakrabarty, and S. Karmakar, Soft Matter **13**, 6929 (2017).
[29] W. Kob, S. Roldn-Vargas, and L. Berthier, Nat. Phys. **8**, 164 (2012).
[30] C. Brito, G. Parisi, and F. Zamponi, Soft Matter **9**, 8540 (2013).
[31] S. Gokhale, K. Hima Nagamanasa, R. Ganapathy, and A. K. Sood, Nat. Commun. **5**, 4685 (2014).
[32] L. Angelani, M. Paoluzzi, G. Parisi, and G. Ruocco, Proc. Natl. Acad. Sci. U.S.A. **115**, 8700 (2018).
[33] S. Torquato, *Random Heterogeneous Materials. Microstructure and Macroscopic Properties* (Springer, New York, 2002).
[34] D. C. Hofmann, J. Y. Suh, A. Wiest, G. Duan, M. L. Lind, M. D. Demetriou, and W. L. Johnson, Nature (London) **451**, 1085 (2008).
[35] R. Dasgupta, P. Mishra, I. Procaccia, and K. Samwer, Appl. Phys. Lett. **102**, 191904 (2013).
[36] O. Gendelman, A. Joy, P. Mishra, I. Procaccia, and K. Samwer, Acta Mater. **63**, 209 (2014).
[37] E. R. Homer, Acta Mater. **83**, 203 (2015).

[38] B. Tyukodi, C. A. Lemarchand, J. S. Hansen, and D. Vandembroucq, Phys. Rev. E **93**, 023004 (2016).
[39] G. R. Garrett, M. D. Demetriou, J. Chen, and W. L. Johnson, Appl. Phys. Lett. **101**, 241913 (2012).
[40] P. H. Tsai, K. T. Hsu, J. H. Ke, H. C. Lin, J. S. C. Jang, and J. C. Huang, Mater. Technol. **30**, 162 (2015).
[41] S. González, J. Mater. Res. **31**, 76 (2016).
[42] L. Jiang, J. K. Li, P. M. Cheng, G. Liu, R. H. Wang, B. A. Chen, J. Y. Zhang, J. Sun, M. X. Yang, and G. Yang, Sci. Rep. **4**, 3605 (2015).
[43] R. Brüning, D. A. St-Onge, S. Patterson, and W. Kob, J. Phys. Condens. Matter **21**, 035117 (2009).
[44] See Supplemental Material at http://link.aps.org/supplemental/10.1103/PhysRevLett.123.185501 for additional description and analysis, and also refer to Refs. [45–50].
[45] A. Lemaitre, J. Chem. Phys. **149**, 104107 (2018).
[46] E. DeGiuli, Phys. Rev. Lett. **121**, 118001 (2018).
[47] S. Henkes and B. Chakraborty, Phys. Rev. E **79**, 061301 (2009).
[48] R. Dasgupta, H. G. E. Hentschel, and I. Procaccia Phys. Rev. Lett. **109**, 255502 (2012).
[49] P. K. Leishangthem, A. D. S. Parmar, and S. Sastry, Nat. Commun. **8**, 14653 (2017).
[50] D. Ganapathi, K. H. Nagamanasa, A. K. Sood, and R. Ganapathy, Nat. Commun. **9**, 397 (2018).
[51] W. Weibull, Proc. R. Swed. Acad. Eng. Sci. **151**, 1 (1939).
[52] W. Kob and D. Coslovich, Phys. Rev. E **90**, 052305 (2014).
[53] A. Barbot, M. Lerbinger, A. Lemaitre, D. Vandembroucq, and S. Patinet, arXiv:1906.09663.
[54] R. L. Moorcroft, M. E. Cates, and S. M. Fielding, Phys. Rev. Lett. **106**, 055502 (2011).
[55] S. Patinet, D. Vandembroucq, and M. L. Falk, Phys. Rev. Lett. **117**, 045501 (2016).
[56] A. Nicolas, E. E. Ferrero, K. Martens, and J.-L. Barrat, Rev. Mod. Phys. **90**, 045006 (2018).
[57] S. P. Niblett, V. K. de Souza, R. L. Jack, and D. J Wales, J. Chem. Phys. **149**, 114503 (2018).
[58] M. Ozawa, A. Ikeda, K. Miyazaki, and W. Kob, Phys. Rev. Lett. **121**, 205501 (2018).
[59] P. Chaudhuri, L. Berthier, and L. Bocquet, Phys. Rev. E **85**, 021503 (2012).